Subband structures and exciton and impurity states in V-shaped GaAs-$Ga_{1-x}Al_xAs$ quantum wires

Zhen-Yan Deng*
Synergy Ceramics Laboratory, Fine Ceramics Research Association & National Industrial Research Institute of Nagoya, 1-1 Hirate-cho, Kita-ku, Nagoya 462-8510, Japan
and Korea Institute for Advanced Study, 207-43 Cheongryangri-dong, Dongdaemun-gu, Seoul 130-012, Republic of Korea

Xiaoshuang Chen
Korea Institute for Advanced Study, 207-43 Cheongryangri-dong, Dongdaemun-gu, Seoul 130-012, Republic of Korea

Tatsuki Ohji
Synergy Ceramics Laboratory, National Industrial Research Institute of Nagoya, 1-1 Hirate-cho, Kita-ku, Nagoya 462-8510, Japan

Takayoshi Kobayashi
Department of Physics, School of Science, University of Tokyo, 7-3-1 Hongo, Bunkyo-ku, Tokyo 113, Japan
(Received 17 May 1999; revised manuscript received 11 January 2000)

The subband structures and exciton and impurity states in V-shaped GaAs-$Ga_{1-x}Al_xAs$ quantum wires (V-QWRs) are investigated by a coordinate transformation method with a variational procedure. The results show that the subband gaps are proportional to the curvature of V-shaped boundaries. Some ''forbidden'' transitions between electrons and heavy holes are found, due to lack of the inversion symmetry for V-QWRs. The exciton binding energies are different for different exciton transitions depending on the localization of exciton states. The theoretical exciton peaks are in good agreement with the recent experimental photoluminescence excitation (PLE) spectra [Phys. Rev. Lett. **78**, 1580 (1997)]. The results also show that there is an asymmetrical distribution of impurity binding energy along the direction normal to the V-shaped boundaries. The impurity position corresponding to maximum binding energy deviates from the center, depending on the dimension and curvature of V-QWRs. The variation in impurity binding energy with impurity position is discussed.

I. INTRODUCTION

In the past few years, there has been an increasing interest in one-dimensional quantum wires,[1] due to the rapid development in material-growth techniques. As the quantum confinement leads to the enhancement of the density of states at specific energies and increases the importance of excitonic effects by the modification of electron-hole Coulomb interaction,[2–4] one-dimensional quantum wire structures have wide potential applications in future optical devices.

V-QWR is a type of typical quantum wire structure, which has attracted considerable attention for over ten years, since the pioneer work of Kapon *et al.*[5,6] The experimental researches on V-QWRs are wide and intensive, including the growth dynamics,[7,8] photoluminescence (PL), and PLE spectra,[9,10] exciton recombination dynamics,[11,12] and electric transport,[13] etc. Vouilloz *et al.*[9] fabricated high-quality V-QWR structures and observed exciton transitions and polarization anisotropy related to multisubbands and valence-band mixing by PLE spectra. Weman *et al.*[10] investigated the PLE spectra in asymmetrical double V-QWRs and demonstrated the electron tunneling and coupling effects between the quantum wires. Arakawa *et al.*[11] studied the quantum confinement Stark effect in V-QWR and found a blueshift of PL peak with the increase of electric fields. In order to explain and explore the physical phenomena in V-QWRs, a number of theoretical methods are adopted, such as the tight-binding method,[14] effective bond-orbital models,[15] plane-wave expansion,[16,17] adiabatic approaches,[18] and envelope function schemes with the finite element,[9,19,20] etc. Rossi *et al.*[16,17] studied the exciton confinement in V-QWRs by the plane-wave expansion, and found that electron-hole Coulomb correlation removes the one-dimensional band-edge singularities from the absorption spectra. They also found that in the strong confinement limit the same potential-to-kinetic energy ratio holds for quite different wire cross sections and compositions. Vouilloz *et al.*[9] used the finite-element method and considered the valence-band mixing effects to calculate the subband transitions in V-QWRs, and their numerical results explained the polarization anisotropy of PLE spectra in V-QWRs. Chang and Xia[20] calculated the quantum stark effects in V-QWRs by the finite-element method, the theoretical Stark shifts are qualitatively in agreement with the experimental measurement. Among these methods, it is not easy to get a simple and intuitive electronic wave function, due to the V-shaped boundaries.

Recently, a coordinate transformation method[21–23] was used to study the electronic structures around corrugated interfaces and in V-QWRs. By this method, the nonplanar boundaries become a confining potential and the boundary conditions of electronic wave functions can be satisfied exactly on the interfaces after the coordinate transformation. In this way, the wave functions are more intuitive and easy to be chosen, compared to other theoretical methods. Inoshita

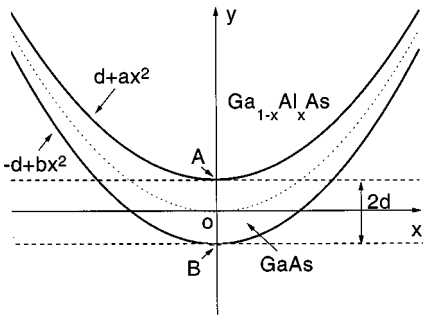

FIG. 1. A schematic representation of V-QWRs, where $d+ax^2$ and $-d+bx^2$ are the upper and bottom boundaries, respectively. The dotted line represents the middle line $y=(a+b)x^2/2$ of V-QWRs, and the dashed lines represent the new boundaries after the coordinate transformation.

and Sakaki[22] have used the coordinate transformation and finite element calculation to study the subband structures in V-QWRs, and their theoretical exciton peak is in good agreement with the experimental PL spectra. However, their coordinate transformation can be used only for some special cases and the lowest exciton transition peak is compared with the experimental spectra. Sun[23] adopted a more generalized coordinate transformation to study the subband structures and Stark effects in V-QWRs, and large Stark shifts in intersubband transitions are predicted. But in Sun's work, only the lowest subbands are calculated and no experimental results are compared. In this paper, the coordinate transformation method with a variational procedure is proposed to investigate all the subband levels, exciton transitions, and impurity binding energies in V-QWRs. Our calculated theoretical exciton peaks are in good agreement with the recent PLE spectra with multisubband exciton transitions, which implies that the method used in this paper probably can be effectively applied to study other physical problems in V-QWRs and other low-dimensional structures with nonplanar interfaces. In Sec. II, the theoretical framework is outlined. The results and discussion are presented in Sec. III.

II. THEORY

A schematic representation of V-QWR is shown in Fig. 1. In the effective-mass approximation within envelope function formalism, the single-particle (electron and hole) Hamiltonian can be written

$$H(\mathbf{r})=\begin{cases}\mathbf{P}^2/(2m_1) & -d+f_2(x)<y<d+f_1(x)\\ \mathbf{P}^2/(2m_2)+V_0 & \text{elsewhere,}\end{cases} \tag{1}$$

where $\mathbf{r}$ and $\mathbf{P}$ are the electron coordinate and momentum; m_1 and m_2 are the carrier-band effective mass in the well material and the barrier material; V_0 is the carrier-confining potential; $d+f_1(x)$ and $-d+f_2(x)$ describe the upper and bottom boundaries of V-QWR, respectively.

The following coordinate transformation transforms the V-shaped boundaries into planar ones

$$x'=x,$$

$$y'=\frac{d}{2d+[f_1(x)-f_2(x)]}\{2y-[f_1(x)+f_2(x)]\}, \tag{2}$$

$$z'=z.$$

After the coordinate transformation, the confining potential becomes

$$V(\mathbf{r}')=\begin{cases}0 & |y'|<d\\ V_0 & \text{elsewhere,}\end{cases} \tag{3}$$

and

$$E=\frac{\int \psi^*(\mathbf{r})H(\mathbf{r})\psi(\mathbf{r})dV}{\int \psi^*(\mathbf{r})\psi(\mathbf{r})dV}$$

$$=\frac{\int \psi^*(\mathbf{r}')|J(\mathbf{r}')|H(\mathbf{r}')\psi(\mathbf{r}')dV'}{\int \psi^*(\mathbf{r}')|J(\mathbf{r}')|\psi(\mathbf{r}')dV'}, \tag{4}$$

where $J(\mathbf{r}')$ is the Jacobian determinant. In fact, in the new coordinate space, the V-QWR becomes a quantum well with a confining potential in the x direction. The electron motion along the wire is a plane wave, and the subband levels in the x-y plane can be obtained by solving the following secular equation:

$$\sum_{m'n'}[\langle mn|J(\mathbf{r}')H(\mathbf{r}')|m'n'\rangle - E_{xy}\langle mn|J(\mathbf{r}')|m'n'\rangle]C_{m'n'}=0, \tag{5}$$

where

$$\psi(x',y')=\sum_{mn} C_{mn}\phi_m(x')\phi_n(y'), \tag{6}$$

and $\phi_m(x')$, $\phi_n(y')$ are two sets of complete basis functions in the x,y directions.

In this paper, two parabolas are used to fit the upper and bottom boundaries of V-QWR. It was found that after the coordinate transformation, the confining potential due to V-shaped boundaries is an harmoniclike potential in the x direction. Therefore, the eigenfunctions of the harmonic oscillator are selected as the basis wave functions in the x direction, that is,

$$\phi_m(x')=N_m e^{-a_n^2 x'^2/2}H_m(\alpha_n x'), \quad m=0,1,2,\ldots, \tag{7}$$

where n is the index of the eigenstates of the quantum well in the y direction (y-QW), N_m is the normalization constant, and $H_m(\alpha_n x')$ is the Hermitian polynomial. The basis wave functions in the y direction are the eigen-wave functions of the quantum well, which include all the confined states[24] and the above-barrier states. In our practical calculation, the states above the barrier are treated as the eigenstates of a big quantum well above the barrier with infinite confining potential,

$$\phi(y)=N\begin{cases}(1+\beta)\cos[k_2y-(k_1-k_2)d]+(1-\beta)\cos[k_2y+(k_1+k_2)d] & -l_0<y<-d\\ 2\cos k_1y \quad |y|<d\\ (1+\beta)\cos[k_2y+(k_1-k_2)d]+(1-\beta)\cos[k_2y-(k_1+k_2)d] & d<y<l_0\end{cases}$$

for even parity states, (8a)

$$\phi(y)=N\begin{cases}(1+\beta)\sin[k_2y-(k_1-k_2)d]-(1-\beta)\sin[k_2y+(k_1+k_2)d] & -l_0<y<-d\\ 2\sin k_1y \quad |y|<d\\ (1+\beta)\sin[k_2y+(k_1-k_2)d]-(1-\beta)\sin[k_2y-(k_1+k_2)d] & d<y<l_0\end{cases}$$

for odd parity states, (8b)

$$k_1=\sqrt{2m_1E/\hbar^2}, \quad k_2=\sqrt{2m_2(E-V_0)/\hbar^2}, \quad \beta=m_2k_1/(m_1k_2), \tag{8c}$$

where N is the normalization constant; E is the discrete level of the big quantum well above the barrier, which can be obtained by the quantum-mechanics boundary conditions. The width $2l_0$ of the big quantum well is selected to be approximate to the electronic coherent length.[25] From the Hamiltonian in the new space, it is found that the harmonic-like potential in the x direction depends on the kinetic energy of the electrons in the y direction. This means the electrons feel different confinement effects due to V-shaped boundaries for the electrons with different kinetic energy in the y direction, and therefore α_n in Eq. (7) is different for different states in y-QW. α_n is determined by minimizing the ground energy level in V-QWR, step by step, by increasing the states in the y direction. In general, 15 basis wave functions in the x direction are used, and we found that it is sufficient to get a good convergent result when the number of the basis wave functions in the y direction increases up to six. Moreover, the eigenfunctions of the system are simple, they usually include a main term and few of the neighboring terms, because the basis wave functions we used are close to the exact solutions to the system. The simple wave functions are helpful to solve some of the other complicated physical problems in V-QWRs.

If two V-shaped boundaries with the same curvatures are considered ($k=a=b$) and the couplings between different states in the y direction are neglected, the subband levels can be obtained analytically

$$E_{mn}=\hbar\omega_n\left(m+\frac{1}{2}\right)+E_{ny}, \quad m=0,1,2,\ldots, \quad n=1,2,\ldots, \tag{9}$$

where

$$\omega_n=2k(2d_nf_n/m_1)^{1/2}, \tag{10a}$$

$$d_n=\begin{cases}1+\left[\left(\frac{m_1}{m_2}-1\right)\frac{1}{k_{2n}}\cos^2k_{1n}d\right]\Big/\left(d+\frac{1}{2k_{1n}}\sin 2k_{1n}d+\frac{1}{k_{2n}}\cos^2k_{1n}d\right) & \text{for odd } n\\ 1+\left[\left(\frac{m_1}{m_2}-1\right)\frac{1}{k_{2n}}\sin^2k_{1n}d\right]\Big/\left(d-\frac{1}{2k_{1n}}\sin 2k_{1n}d+\frac{1}{k_{2n}}\sin^2k_{1n}d\right) & \text{for even } n,\end{cases} \tag{10b}$$

$$f_n=\begin{cases}E_{ny}-\left[V_0\frac{1}{k_{2n}}\cos^2k_{1n}d\right]\Big/\left(d+\frac{1}{2k_{1n}}\sin 2k_{1n}d+\frac{1}{k_{2n}}\cos^2k_{1n}d\right) & \text{for odd } n\\ E_{ny}-\left[V_0\frac{1}{k_{2n}}\sin^2k_{1n}d\right]\Big/\left(d-\frac{1}{2k_{1n}}\sin 2k_{1n}d+\frac{1}{k_{2n}}\sin^2k_{1n}d\right) & \text{for even } n\end{cases} \tag{10c}$$

$$k_{1n}^2=2m_1E_{ny}/\hbar^2, \quad k_{2n}^2=2m_2(V_0-E_{ny})/\hbar^2. \tag{10d}$$

Here, E_{ny} is the subband level of y-QW.[24] In Eq. (9), it is apparent that the subband levels and subband gaps are proportional to the curvature of V-shaped boundaries. The above analytical equations can be used to evaluate the subband structures in practical V-QWRs approximately.

The Hamiltonians for exciton[20,26,27] and shallow donor impurity[24] states in V-QWRs can be written

$$H_{e-h}(\mathbf{r})=H_e(x_e,y_e)+H_h(x_h,y_h)+V_{e-h}(\mathbf{r})$$
$$+\begin{cases} -\dfrac{\hbar^2\partial^2}{2\mu_{11}\partial z^2} & -d+f_2(x_e)<y_e<d+f_1(x_e),\quad -d+f_2(x_h)<y_h<d+f_1(x_h) \\ -\dfrac{\hbar^2\partial^2}{2\mu_{12}\partial z^2} & -d+f_2(x_e)<y_e<d+f_1(x_e),\quad y_h<-d+f_2(x_h)\ \text{ or }\ >d+f_1(x_h) \\ -\dfrac{\hbar^2\partial^2}{2\mu_{21}\partial z^2} & y_e<-d+f_2(x_e)\ \text{ or }\ >d+f_1(x_e),\quad -d+f_2(x_h)<y_h<d+f_1(x_h) \\ -\dfrac{\hbar^2\partial^2}{2\mu_{22}\partial z^2} & y_e<-d+f_2(x_e)\ \text{ or }\ >d+f_1(x_e),\quad y_h<-d+f_2(x_h)\ \text{ or }\ >d+f_1(x_h), \end{cases} \tag{11a}$$

$$H_{im}(\mathbf{r})=V_{\text{ion}}(\mathbf{r})+\begin{cases}\mathbf{P}^2/(2m_{1e}) & -d+f_2(x)<y<d+f_1(x)\\ \mathbf{P}^2/(2m_{2e})+V_e & \text{elsewhere,}\end{cases} \tag{11b}$$

where

$$H_\xi(x_\xi,y_\xi)=\begin{cases} -\dfrac{\hbar^2}{2m_{1\xi}}\left(\dfrac{\partial^2}{\partial x_\xi^2}+\dfrac{\partial^2}{\partial y_\xi^2}\right) & -d+f_2(x_\xi)<y_\xi<d+f_1(x_\xi)\\ -\dfrac{\hbar^2}{2m_{2\xi}}\left(\dfrac{\partial^2}{\partial x_\xi^2}+\dfrac{\partial^2}{\partial y_\xi^2}\right)+V_\xi & \text{elsewhere,}\end{cases}$$
$$\xi=e,h \tag{12a}$$

$$V_{e-h}(\mathbf{r})=-\frac{e^2}{\varepsilon[(x_e-x_h)^2+(y_e-y_h)^2+z^2]^{1/2}}, \tag{12b}$$

$$\mu_{ij}=\frac{m_{ie}m_{jh}}{m_{ie}+m_{jh}},\quad i,j=1,2, \tag{12c}$$

$$V_{\text{ion}}(\mathbf{r})=-e^2/(\varepsilon|\mathbf{r}-\mathbf{r}_0|). \tag{12d}$$

Here, ε is the dielectric constant, and the difference in dielectric constant between the well material and barrier material is neglected. $\mathbf{r}_0$ is the impurity position in V-QWRs.

The exciton and impurity binding energies in V-QWRs are calculated by a traditional variational method, due to no exact solutions to the exciton and impurity states in quantum wires. The following trial wave functions in the new coordinate space are adopted for the exciton[20,28] and ground impurity states[29–35] in V-QWRs:

$$\psi_{e-h}(\mathbf{r}')=\psi(x_e',y_e')\,\psi(x_h',y_h')\exp(-\gamma z'^2), \tag{13}$$

and

$$\psi(\mathbf{r}')=\psi_0(\mathbf{r}')\exp(-\lambda|\mathbf{r}'-\mathbf{r}_0'|), \tag{14}$$

where $\psi(x_e',y_e')$ and $\psi(x_h',y_h')$ are the related electron and hole subband wave functions; $\mathbf{r}_0'$ is the impurity position after the coordinate transformation and $\psi_0(\mathbf{r}')$ is the ground electronic wave function in V-QWRs; γ and λ are the variational parameters. The above trial wave functions satisfy the boundary conditions exactly on the interfaces.

The exciton binding energies for different exciton transitions and the ground impurity binding energy in V-QWRs are obtained as follows:

$$E_{e-h}=E_e+E_h-\min_\gamma\langle\psi_{e-h}(\mathbf{r}')|J(\mathbf{r}')\times H_{e-h}(\mathbf{r}')|\psi_{e-h}(\mathbf{r}')\rangle/\langle\psi_{e-h}(\mathbf{r}')|\times J(\mathbf{r}')|\psi_{e-h}(\mathbf{r}')\rangle, \tag{15}$$

and

$$E_b=E_0-\min_\lambda\langle\psi(\mathbf{r}')|J(\mathbf{r}')\times H_{im}(\mathbf{r}')|\psi(\mathbf{r}')\rangle/\langle\psi(\mathbf{r}')|J(\mathbf{r}')|\psi(\mathbf{r}')\rangle, \tag{16}$$

where E_e and E_h are the electronic and hole subband levels, E_0 is the ground electronic level in V-QWRs; $H_{e-h}(\mathbf{r})$ and $H_{im}(\mathbf{r}')$ are the exciton and impurity state Hamiltonians in the new coordinate space, respectively. The above integrals were calculated numerically.

III. RESULTS AND DISCUSSION

A. Exciton transitions

In order to test the feasibility of our theoretical method, the theoretical results are compared with the recent experimental PLE spectra by Vouilloz *et al.*[9] First of all, we measure the boundaries from the TEM micrograph of V-QWR specimen, and then fit the upper and bottom boundaries by two different parabolas. The inset in Fig. 2(b) indicates that parabola is a good function to fit the V-shaped boundaries.

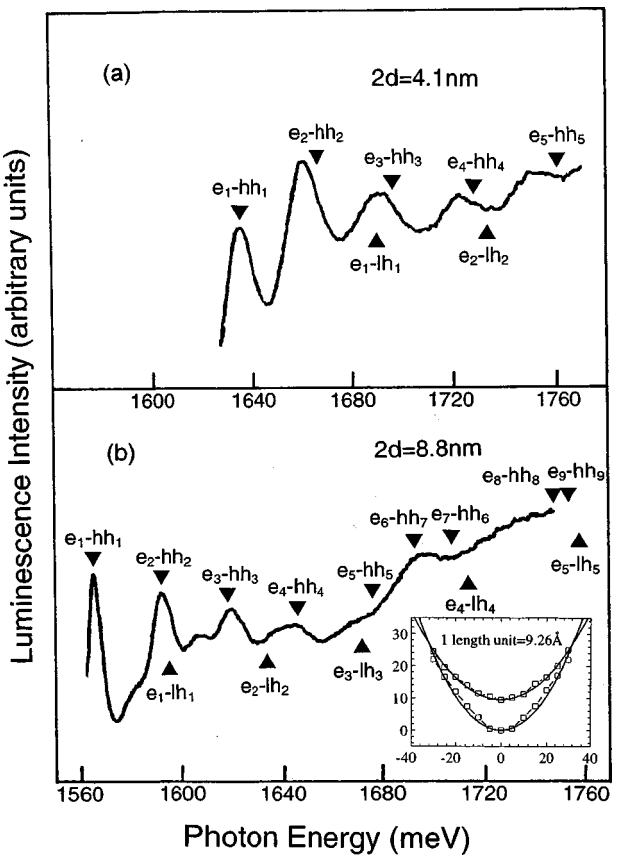

FIG. 2. Comparison between the calculated exciton transition peaks (arrows) and the experimental PLE spectra in Ref. 9 (solid lines) for the $GaAs/Ga_{0.7}Al_{0.3}As$ V-QWRs with the width of (a) $2d=4.1$ nm and (b) $2d=8.8$ nm, where the polarized direction of the light is parallel to the quantum wire. The inset in (b) represents the measured upper and bottom boundaries (open squares and dashed lines) and the fitting boundaries (solid lines) of the 8.8-nm V-QWR.

As the curvature is different for the upper and bottom fitting parabolas, and two parabolas will cross somewhere. In the model calculation, the cross section of the quantum wire is closed (the x integral region is between two cross points). But this does not affect the calculated results much, because there is some necking existed between the bottom quantum wire and the side quantum well in the experimental specimen (Fig. 1 of Ref. 9). The material parameters[36] and the fitting curvatures for two different V-QWRs in Ref. 9 are listed in Table I.

Table II gives the main exciton transitions and exciton binding energies in two different V-QWRs,[9] where the mixing between the heavy-hole and light-hole states is not considered. One reason is this paper focuses on the theoretical method to deal with the subband structures in V-QWRs. Another reason is, the mixing of heavy-hole and light-hole states only affects the weak structures in the optical absorption spectra in low-dimensional systems,[37,38] and the effects of valence-band mixing on exciton binding energies is very small.[39] Moreover, only the exciton transitions for the incident light with the polarized direction parallel to the quantum wire are considered in this work. In the quantum wire direction the lattice translational symmetry holds as bulk materials. Of course, valence-band mixing in V-QWRs is an interesting problem, and is important for the transitions with the light of the polarized direction normal to the quantum wire. We will study this problem in a forthcoming paper. Table II shows that, the transition condition $\Delta l=l_e-l_h=0$ (l is the index of the electron and hole eigenstates) is not always observed, and some ''forbidden'' transitions are found, for example, the e_6-hh_7 and e_7-hh_6 transitions for 8.8-nm V-QWR. Actually, the $\Delta l\neq 0$ transitions in 8.8-nm V-QWR is a result of the different coupling of the confined states in the y direction with those in the x direction for the electron and heavy hole. This is because there are two confined electronic states in the y-QW for 8.8-nm V-QWR, and the coupling between the states of x and y directions are strong around the second level of the y-QW. This coupling is different for the electron and heavy-hole states, due to the lack of the inversion symmetry for the V-QWR in the y direction, that is, e_6 and hh_7 have the same symmetry, e_7 and hh_6 have the same symmetry. But for 4.1-nm V-QWR, the situation is different, because it has only one confined electronic state in the y-QW, and the coupling of the states in the x and y direction is monotonous. Therefore, no ''forbidden'' transitions appear. Table II also shows that, the exciton binding energy is different for different exciton transitions. The value of exciton binding energy depends on the localization of the subband states. Usually, the localization of subband eigenstates in V-QWRs weakens when their index increases, and the exciton binding energy is smaller for the higher exciton

TABLE I. The parameters of V-QWRs used in the calculations.

Parameter	Value
energy gap in $Ga_{1-x}Al_xAs$ (E_g^{GaAlAs})	$E_g^{GaAs}+1.247x$ eV
band offsets ($\Delta E_c/\Delta E_v$)	65/35
electron effective mass in $Ga_{1-x}Al_xAs$ (m_{e2})	$(0.067+0.083x)m_0$
heavy-hole effective mass in $Ga_{1-x}Al_xAs$ (m_{hh2})	$(0.51+0.25x)m_0$
light-hole effective mass in $Ga_{1-x}Al_xAs$ (m_{lh2})	$(0.082+0.068x)m_0$
dielectric constant (ε)	12.6
curvature of the upper boundary (a)	0.0269 nm^{-1} for 4.1-nm V-QWR
	0.0184 nm^{-1} for 8.8-nm V-QWR
curvature of the bottom boundary (b)	0.0283 nm^{-1} for 4.1-nm V-QWR
	0.0283 nm^{-1} for 8.8-nm V-QWR
width of the big quantum well above barrier ($2l_0$)	120 nm

TABLE II. The exciton binding energy for different electron-hole transitions in two different V-QWRs.

$2d=4.1$ nm		$2d=8.8$ nm	
$E_{e\text{-}hh}$ (meV)	$E_{e\text{-}lh}$ (meV)	$E_{e\text{-}hh}$ (meV)	$E_{e\text{-}lh}$ (meV)
16.55 (e_1-hh_1)	12.76 (e_1-lh_1)	12.24 (e_1-hh_1)	11.07 (e_1-lh_1)
12.96 (e_2-hh_2)	9.52 (e_2-lh_2)	10.43 (e_2-hh_2)	8.74 (e_2-lh_2)
10.99 (e_3-hh_3)	8.44 (e_3-lh_3)	9.14 (e_3-hh_3)	7.83 (e_3-lh_3)
10.46 (e_4-hh_4)	7.77 (e_4-lh_4)	8.58 (e_4-hh_4)	7.19 (e_4-lh_4)
5.70 (e_5-hh_5)		8.30 (e_5-hh_5)	6.90 (e_5-lh_5)
		13.16 (e_6-hh_7)	9.91 (e_6-lh_6)
		7.79 (e_7-hh_6)	6.57 (e_7-lh_7)
		7.60 (e_8-hh_8)	
		8.89 (e_9-hh_9)	
		8.81 (e_9-hh_{10})	

transitions. However, the e_6 and hh_7 states in 8.8-nm V-QWR consist mainly of the second y confined state and the first x harmonic state, and the localization of e_6-hh_7 exciton is not weaker than that of e_1-hh_1 exciton. This causes the e_6-hh_7 exciton to have higher exciton binding energy.

The comparison of the theoretical exciton peaks to the experimental PLE spectra for two different V-QWRs is shown in Fig. 2, where the theoretical exciton peaks $E_{\text{peak}}=E_g^{\text{GaAs}}+E_e+E_h-E_{e-h}$, and E_g^{GaAs} is the energy gap of bulk GaAs. The GaAs energy gap E_g^{GaAs} is determined by fitting the first theoretical e_1-hh_1 peak to the first experimental PLE peak, and we get $E_g^{\text{GaAs}}=1505.8$ meV for 4.1-nm V-QWR and 1518.3 meV for 8.8-nm V-QWR. The energy gap of bulk GaAs that we obtained for 8.8-nm V-QWR is almost the same as that of Vouilloz *et al.*[9] From Fig. 2, it can be seen that the theoretical exciton peaks are in good agreement with those of the experimental PLE spectra, especially for 8.8-nm V-QWR. The small difference for 4.1-nm V-QWR may be due to the small structure difference used in the theoretical calculation and that in the experiment, as no TEM micrograph can be available for the 4.1-nm V-QWR. Vouilloz *et al.*[9] calculated the transition peaks excluding exciton effects (let the exciton binding energies be a constant for different exciton transitions) by finite element method, and found that their theoretical peaks are overall in good agreement with those of the experimental PLE spectra. If the exciton effects are considered, their theoretical peaks will be shifted towards the high-energy side, especially for 4.1-nm V-QWR. Because the exciton binding energy usually decreases with the increase in the index of exciton transitions, as listed in Table II, and the difference in exciton binding energy for different transitions is not small. For example, this difference is over 10 meV between e_1-hh_1 and e_5-hh_5 excitons in 4.1-nm V-QWR. It is apparent that our theoretical exciton peaks are more close to the experimental PLE peaks, compared to those by the finite element method, if different exciton binding energy for different transition is considered in finite element method. Figure 3 shows the square of the optical matrix elements[9] for different exciton transitions in two different V-QWRs, where

$$|M|^2=|\langle\psi_c(\mathbf{r})|\psi_V(\mathbf{r})\rangle|^2|\langle u_c(\mathbf{r})|\mathbf{e}\cdot\mathbf{P}|u_V(\mathbf{r})\rangle|^2$$

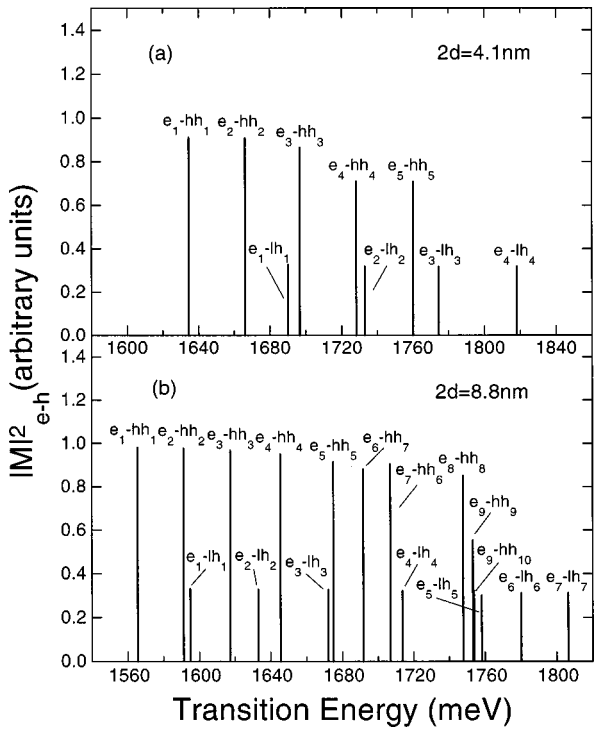

FIG. 3. Square of the optical matrix elements for the heavy- and light-hole exciton transitions in (a) 4.1-nm and (b) 8.8-nm V-QWRs, where the polarized direction of the light is parallel to the quantum wire.

and we deal with the difference for the heavy-hole and light-hole transitions by a conclusion of Chang *et al.*,[37] that is,

$$|\langle u_c(\mathbf{r})|P_z|u_{hh}(\mathbf{r})\rangle|^2=3|\langle u_c(\mathbf{r})|P_z|u_{lh}(\mathbf{r})\rangle|^2.$$

Therefore, the PLE spectra shown in figure 2 reflect mainly the information of heavy-hole exciton transitions.

B. Impurity states

The impurity states are an important factor to affect the electric-transportation and optical properties in low-dimensional semiconductor structures. As no experimental results for impurity states in V-QWRs can be available, an ideal situation will be considered here. Figures 4(a)–5(a) show the variations in impurity binding energy with the dimension and curvature of V-QWRs for three different impurity positions, respectively, where O is the center of V-QWRs, A and B are the cross points of the upper and bottom V-shaped boundaries with y axis (see Fig. 1). Here, the upper and bottom boundaries with the same curvatures ($a=b$) are considered, as in most cases, two boundaries of V-QWRs do not cross each other in the experiments.[6–11] The variation ranges of the dimension and curvature of V-QWRs we adopted in Figs. 4 and 5 have been realized in the experiments.[6–11] From Fig. 4(a), it can be seen that when the dimension of V-QWRs decreases, the impurity binding energy at three different points increases at first, to a peak value, and then decreases, which are similar to the impurity state behavior in traditional quantum wires with finite confining potential.[30,33] This phenomenon is related to the

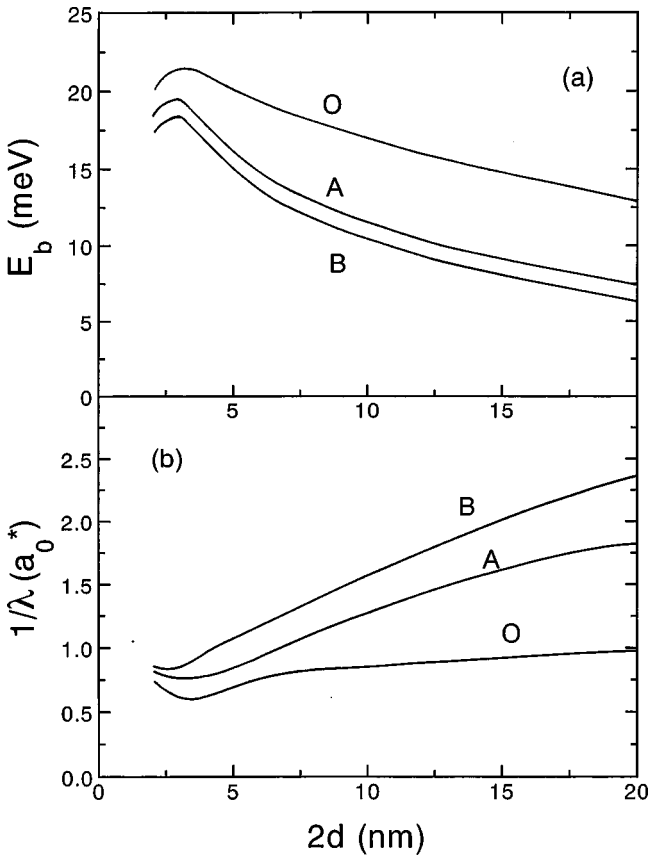

FIG. 4. Variations in (a) impurity binding energy and (b) the variational parameter of ground impurity trial wave function with the dimension of V-QWRs for three different impurity positions shown in Fig. 1. The Al composition in barrier material is $x=0.4$ and the curvatures of V-shaped boundaries are $a=b=0.04\,\mathrm{nm}^{-1}$.

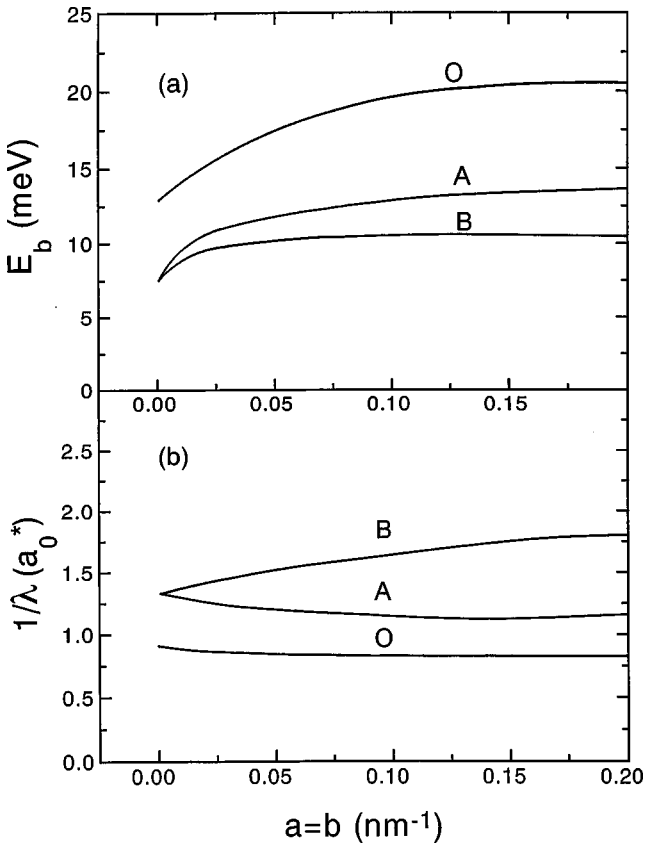

FIG. 5. Variations in (a) impurity binding energy and (b) the variational parameter of ground impurity trial wave function with the curvature of V-shaped boundaries for three different impurity positions shown in Fig. 1. The Al composition in barrier material is $x=0.4$ and the dimension of V-QWRs is $2d=10$ nm.

change of the electron confinement in V-QWRs. When the dimension of V-QWRs decreases, the confinement of electrons is strengthened, and therefore the impurity binding energy increases. Because the practical V-QWRs with finite confining potential are considered here, and when the dimension of V-QWRs is reduced to a small limited value, most of the electronic wave functions begin to leak out of the GaAs well material, which results in a peak impurity binding energy at a small $2d$ value. In Fig. 4(a), it can be also seen that the impurity binding energy at the center is larger than that at two boundary points. The impurity binding energy at the upper boundary point is larger than that at bottom boundary point, which indicates an asymmetrical distribution of impurity binding energy along the direction normal to the boundaries. This difference is different from the impurity state behavior in traditional quantum wire structures.[29,30,33] As stated in Sec. II, the effect of two V-shaped boundaries on the electron motion in the x direction can be viewed as a confining potential, but this confining potential is asymmetrical in the y direction. From the geometry of V-QWRs, it is apparent that most of the electronic wave functions are pushed towards the convex side in the well, due to the shape of the barrier boundaries. This implies that the electronic wave functions are asymmetrical in the y direction, and the weighted center of electronic wave functions moves towards the convex side in the well. Therefore, the impurity binding energy at two boundary cross points is different. When the curvature of the V-shaped boundary increases, the confining potential in the x direction increases, which causes the impurity binding energy to increase, as shown in Fig. 5(a). At the same time, the increase in the curvature of V-shaped boundary increases the asymmetry of the confining potential in the y direction, and the difference in binding energy between the upper and bottom boundary points increases. The decrease in binding energy at bottom boundary point B for the higher curvature of V-shaped boundary in Fig. 5(a) is related to the serious leakage of the electronic wave function in the well material.

The variations in impurity binding energy with the dimension and curvature of V-QWRs can be also explained by the localization of impurity states, as shown in Figs. 4(b)–5(b), where the length is in units of the effective Bohr radius, $a_0^*=\hbar^2\varepsilon/(m_e e^2)$, with m_e being the electron effective mass in GaAs. In a sense, the value $(1/\lambda)$ of the variational parameter in Eq. (14) is a representation of the impurity Bohr radius and the localization of impurity states in V-QWRs. It is apparent that the variations in impurity Bohr radius and impurity state localization in Figs. 4(b)–5(b) are consistent with the variations in impurity binding energy in Figs. 4(a)–5(a). That is, the stronger the localization of impurity states, the larger the impurity binding energy is.

Because of the asymmetrical distribution of the confining potential in the y direction, it is found that the impurity po-

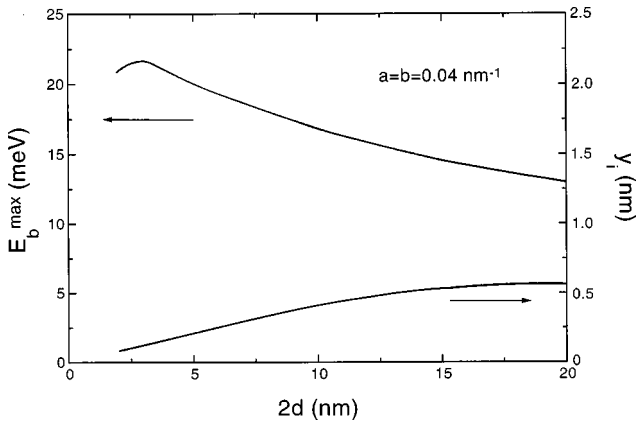

FIG. 6. Dependence of maximum impurity binding energy and its corresponding impurity position ($x_i=0$) on the dimension of V-QWRs where the Al composition in barrier material is $x=0.4$.

sition corresponding to maximum binding energy deviates from the center of V-QWRs. The dependence of maximum impurity binding energy and its corresponding impurity position on the dimension and curvature of V-QWRs are shown in Figs. 6–7. Figures 6 and 7 show that the variations in maximum binding energy with the dimension and curvature of V-QWRs are similar to the results in Figs. 4–5, and the deviation of peak impurity position from the center becomes large as the dimension or curvature of V-QWRs increase.

In order to understand clearly the asymmetrical distribution of impurity binding energy in V-QWRs, Fig. 8 shows the dependence of impurity binding energy on the impurity position along the y axis and the middle line between two V-shaped boundaries. The dashed line in Fig. 8 represents the impurity binding energies in a real V-QWR structure.[9] The asymmetrical distribution of impurity binding energy along the y direction can be clearly seen in Fig. 8(a), and the weighted center of binding energy distribution in the y direction moves to the convex side of V-QWRs. The distribution of impurity binding energy along the middle line is symmetrical, due to the symmetrical boundaries of V-QWRs and its resultant confining potential in the x direction. It is apparent that the impurity binding energy along the middle line

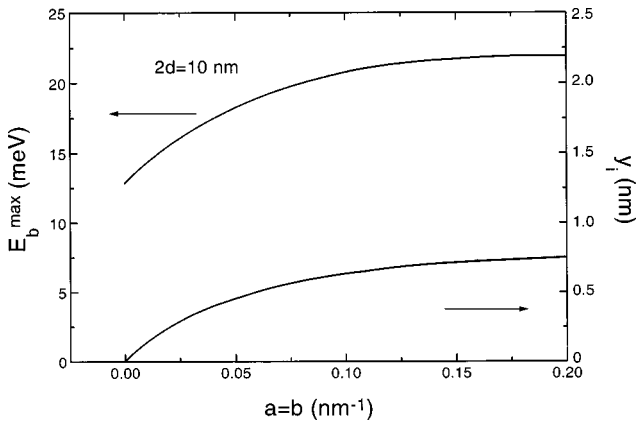

FIG. 7. Dependence of maximum impurity binding energy and its corresponding impurity position ($x_i=0$) on the curvature of V-shaped boundaries, where the Al composition in barrier material is $x=0.4$.

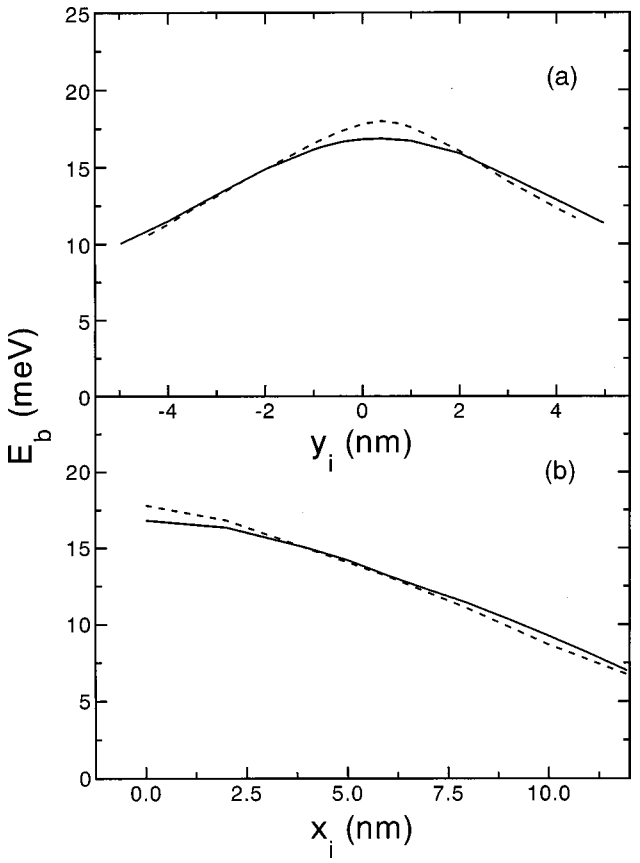

FIG. 8. Variations in impurity binding energy with the impurity position (a) along the y axis ($x_i=0$) and (b) along the middle line (the dotted line shown in Fig. 1) of V-QWRs. The solid line corresponds to a V-QWR with the Al composition in barrier material $x=0.4$, dimension $2d=10$ nm and curvatures $a=b=0.04\ \mathrm{nm}^{-1}$. The dashed line corresponds to a real V-QWR in Ref. 9 with the Al composition in barrier material $x=0.3$, dimension $2d=8.8$ nm and curvatures $a=0.0184\ \mathrm{nm}^{-1}$, $b=0.0283\ \mathrm{nm}^{-1}$.

decreases as the impurity position is away from the center of V-QWRs, as shown in Fig. 8(b), which is similar to the variations in impurity binding energy with the impurity position within the cross section of traditional quantum wire structures.[29–31,33] In addition, the results in Fig. 8 show that the impurity state behavior has no qualitative difference for the V-QWRs in which the upper and bottom boundaries have or have not the same curvature. If other different kinds of functions, which are more exact to describe the V-shaped boundaries, are used, it is believed that the above qualitative results have no change, though there are some small quantitative changes in impurity binding energy in V-QWRs.

In summary, we have studied the subband structures, exciton transitions, and impurity states in V-QWRs by a coordinate transformation method with a variational procedure. It was found that the subband gaps are proportional to the curvature of V-shaped boundaries, and there are some ''forbidden'' transitions that appeared between electrons and heavy holes. The exciton binding energy is different for different exciton transitions depending on the localization of subband states. The theoretical exciton peaks are in good agreement with those of the recent experimental PLE spectra. It was

also found that the impurity state behavior in V-QWRs in a sense is similar to that in traditional quantum wires. However, the distribution of impurity binding energy along the direction normal to the V-shaped boundaries is asymmetrical, and the impurity position corresponding to the maximum binding energy deviates from the center, due to the asymmetrical confining potential produced by the V-shaped boundaries in the *y* direction.

ACKNOWLEDGMENTS

The authors are grateful to Professor K. J. Chang and Professor Steven G. Louie at Berkeley for their helpful suggestions. This work was supported by NEDO in Japan and the QMX Project Foundation of Shanghai Science and Technology in China.

*Electronic address: zydeng@nirin.go.jp

[1] H. Akiyama, J. Phys.: Condens. Matter **10**, 3095 (1998) (and references therein).
[2] T. Ogawa and T. Takagahara, Phys. Rev. B **44**, 8138 (1991).
[3] S. Glutsch and F. Bechstedt, Phys. Rev. B **47**, 4315 (1993).
[4] J. B. Xia and K. W. Cheah, Phys. Rev. B **55**, 1596 (1997).
[5] E. Kapon, M. C. Tamargo, and D. M. Hwang, Appl. Phys. Lett. **50**, 347 (1987).
[6] E. Kapon, D. M. Hwang, and R. Bhat, Phys. Rev. Lett. **63**, 430 (1989).
[7] G. Biasiol, E. Kapon, Y. Ducommun, and A. Gustafsson, Phys. Rev. B **57**, R9416 (1998).
[8] G. Biasiol and E. Kapon, Phys. Rev. Lett. **81**, 2962 (1998).
[9] F. Vouilloz, D. Y. Oberli, M. A. Dupertuis, A. Gustafsson, F. Reinhardt, and E. Kapon, Phys. Rev. Lett. **78**, 1580 (1997); Phys. Rev. B **57**, 12 378 (1998).
[10] H. Weman, D. Y. Oberli, M.-A. Dupertuis, F. Reinhardt, A. Gustafsson, and E. Kapon, Phys. Rev. B **58**, 1150 (1998).
[11] T. Arakawa, Y. Kato, F. Sogawa, and Y. Arakawa, Appl. Phys. Lett. **70**, 646 (1997).
[12] M. Lomascolo, P. Ciccarese, R. Cingolani, R. Rinaldi, and F. K. Reinhart, J. Appl. Phys. **83**, 302 (1998).
[13] D. Kaufman, Y. Berk, B. Dwir, A. Rudra, A. Palevski, and E. Kapon, Phys. Rev. B **59**, R10 433 (1999).
[14] Y. Arakawa, T. Yamauchi, and J. N. Schulman, Phys. Rev. B **43**, 4732 (1991).
[15] D. S. Citrin and Y. C. Chang, IEEE J. Quantum Electron. **29**, 97 (1993).
[16] F. Rossi and E. Molinari, Phys. Rev. Lett. **76**, 3642 (1996).
[17] F. Rossi, G. Goldoni, and E. Molinari, Phys. Rev. Lett. **78**, 3527 (1997).
[18] C. Ammann, M. A. Dupertuis, U. Bockelmann, and B. Deveaud, Phys. Rev. B **55**, 2420 (1997).
[19] O. Stier and D. Bimberg, Phys. Rev. B **55**, 7726 (1997).
[20] K. Chang and J. B. Xia, Phys. Rev. B **58**, 2031 (1998).
[21] Z. Y. Deng, Y. F. Zhang, and J. K. Guo, J. Phys.: Condens. Matter **7**, 6483 (1995).
[22] T. Inoshita and H. Sakaki, J. Appl. Phys. **79**, 269 (1996).
[23] H. Sun, Phys. Rev. B **58**, 15 381 (1998).
[24] Z. Y. Deng, T. R. Lai, and J. K. Guo, Phys. Rev. B **50**, 5732 (1994).
[25] W. Lu, Y. M. Mu, X. Q. Liu, X. S. Chen, M. F. Wan, G. L. Shi, Y. M. Qiao, S. C. Shen, Y. Fu, and M. Willander, Phys. Rev. B **57**, 9787 (1998).
[26] J. W. Brown and H. N. Spector, Phys. Rev. B **35**, 3009 (1987).
[27] M. H. Degani and O. Hipolito, Phys. Rev. B **35**, 9345 (1987).
[28] Y. C. Chang, L. L. Chang, and L. Esaki, Appl. Phys. Lett. **47**, 1324 (1985).
[29] G. W. Bryant, Phys. Rev. B **29**, 6632 (1984); **31**, 7812 (1985).
[30] J. W. Brown and H. N. Spector, J. Appl. Phys. **59**, 1179 (1986).
[31] G. Weber, P. A. Schulz, and L. E. Oliveira, Phys. Rev. B **38**, 2179 (1993).
[32] S. V. Branis, G. Li, and K. K. Bajaj, Phys. Rev. B **47**, 1316 (1993).
[33] Z. Y. Deng, T. R. Lai, J. K. Guo, and S. W. Gu, J. Appl. Phys. **75**, 7389 (1994).
[34] H. T. Cao and D. B. T. Thoai, Physica B **205**, 273 (1995).
[35] A. Montes, C. A. Duque, and N. Porras-Montenegro, J. Phys.: Condens. Matter **10**, 5351 (1998).
[36] H. Kalt, *Optical Properties of III-V Semiconductors* (Springer, New York, 1996), p. 177.
[37] Y. C. Chang and J. N. Schulman, Phys. Rev. B **31**, 2069 (1985).
[38] G. D. Sanders and Y. C. Chang, Phys. Rev. B **31**, 6892 (1985); **32**, 4282 (1985); **35**, 1300 (1987).
[39] B. Zhu and K. Huang, Phys. Rev. B **36**, 8102 (1987).